Structural and Multidisciplinary Optimization (2021) 63:2191–2209
https://doi.org/10.1007/s00158-020-02794-y

RESEARCH PAPER

Crashworthiness analysis and optimization of standard and windowed multi-cell hexagonal tubes

T. N. Tran[1] · Ahmad Baroutaji[2] · Quirino Estrada[3] · Arun Arjunan[2] · HuuSon Le[1] · N. P. Thien[4,5]

Received: 29 June 2020 / Revised: 11 October 2020 / Accepted: 18 November 2020 / Published online: 7 January 2021

Abstract

Recently, multi-cell structures have received increased attention for crashworthiness applications due to their superior energy absorption capability. However, such structures were featured with high peak collapsing force (PCL) forming a serious safety concern, and this limited their application for vehicle structures. Accordingly, this paper proposes windowed shaped cuttings as a mechanism to reduce the high PCL of the multi-cell hexagonal tubes and systemically investigates the axial crushing of different windowed multi-cell tubes and also seeks for their optimal crashworthiness design. Three different multi-cell configurations were constructed using wall-to-wall (WTW) and corner-to-corner (CTC) connection webs. Validated finite element models were generated using explicit finite element code, LS-DYNA, and were used to run crush simulations on the studied structures. The crashworthiness responses of the multi-cell standard tubes (STs), i.e., without windows, and multi-cell windowed tubes (WTs) were determined and compared. The WTW connection type was found to be more effective for STs and less favorable for WTs. Design of experiments (DoE), response surface methodology (RSM), and multiple objective particle swarm optimization (MOPSO) tools were employed to find the optimal designs of the different STs and WTs. Furthermore, parametric analysis was conducted to uncover the effects of key geometrical parameters on the main crashworthiness responses of all studied structures. The windowed cuttings were found to be able to slightly reduce the PCL of the multi-cell tubes, but this reduction was associated with a major negative implication on their energy absorption capability. This work provides useful insights on designing effective multi-cell structures suitable for vehicle crashworthiness applications.

Keywords Crashworthiness optimization · Trigger · Windowed multi-cell tube · Energy absorption · Dynamic collapsing

1 Introduction

Thin-walled tubes have been widely utilized as efficient energy absorbers in vehicles' structural frame to reduce the harmful influences of impact loading and to protect the passengers. Peak collapsing load (PCL) and specific energy absorption (SEA) are the most important responses of energy absorbing structure for vehicle crashworthiness applications. Generally, high SEA and low PCL are preferred to ensure the lightweight design of the vehicle and the safety of the passengers. Over the past years, there was a growing interest in the crashworthiness field where the crush responses and deformation modes of various structures under quasi-static and dynamic loads were investigated using numerical, analytical, and experimental methods (Niknejad and Bonakdar 2015; Niknejad and Orojloo 2016; Zahran et al. 2018; Esa et al. 2017; Estrada et al. 2018a, 2018b, 2019; Taghipoor and Noori Mohammad 2018; Taghipoor and Damghani Nouri 2018a, 2018b; Taghipoor et al. 2020a; Tran et al. 2020; Baroutaji et al. 2021). For example, DiPaolo et al. (2004) carried out an investigation on the compression behavior of steel square tubes under quasi-static loading. Ahmad and Thambiratnam (2009) studied the energy absorption ability

Responsible Editor: Axel Schumacher

✉ N. P. Thien
nguyenphucthien@duytan.edu.vn

[1] Faculty of Automobile Technology, Van Lang University, Ho Chi Minh City, Vietnam

[2] School of Engineering, University of Wolverhampton, Telford Innovation Campus, Telford TF29NT, UK

[3] Institute of Engineering and Technology, Autonomous University of Juarez City (UACJ), Ciudad Juarez, Chihuahua, Mexico

[4] Institute of Research and Development, Duy Tan University, Danang 550000, Vietnam

[5] Faculty of Environmental and Chemical Engineering, Duy Tan University, Danang 550000, Vietnam

of foam-filled conical tubes under impact loading and considered the effects of the geometry and loading angles on the behavior of such structures. Mahdi Abedi et al. (2012) executed crush experiments on empty and foam-filled tubes to develop analytical formulas for predicting folding load. Meran (2016) examined the crashworthiness of thin-walled tubes with different geometrical shapes and revealed the influence of cross-section shape on the crashworthiness metrics. Eyvazian et al. (2020) studied the behavior of the vertical corrugated square tube under axial loading and pointed out that the height of the vertical waves strongly affects the maximum compression load of the tube. Taghipoor et al. (2020b) compared the crashworthiness characteristics of the different energy absorbers in case of low speed loading. Among the different configurations, the aluminum foam-filled square tube showed the better crashworthiness performance.

Recently, multi-cell tubes have received increased research attention as new set of structures with outstanding energy absorption capability, and their crashworthiness performance was the subject of study for many researchers. For instance, Kim (2002) introduced new multi-cell square tubes with better crashworthiness performance than the traditional single-cell configuration. Alavi and Parsapour (2014) and Vimal Kannan and Rajkumar (2020) studied the energy absorption ability of different multi-cell tubes and pointed out that the multi-cell hexagonal and octagonal tubes have better crashworthiness performance than multi-cell square tubes. Xu et al. (2018) conducted crashworthiness analysis on hierarchical hexagonal tubes and explored the main factors affecting their energy absorption responses. Generally, it was reported that a multi-cell tube has better crashworthiness performance than its single-cell counterpart because it can absorb greater SEA (Chen and Wierzbicki 2001). However, the high SEA of the multi-cell tubes is normally associated with a very high PCL which is much greater than its single-cell counterpart.

To reduce PCL of an energy absorber, crush initiators are normally implemented on the tube walls. In addition to reducing the PCL, initiators play a key role in controlling the folding process and inhibiting the undesirable global buckling deformation mode. The crush initiators come in different formats including grooves, corrugations, or holes. El-Hage et al. (2005) studied the effects of the different initiators' mechanisms on the crushing behavior using simulation. Hosseinipour and Daneshi (2003) considered the crashworthiness performance of grooved tubes and showed that such tubes have smaller PCL and better collapsing behavior than those of the corresponding traditional tubes without grooves. Eyvazian et al. (2012, 2014, 2018) examined the effects of the corrugations on the collapsing behavior and crashworthiness indexes including SEA and PCL. The authors reported that the corrugations make the collapsing mode of the tubes more controllable. Alkhatib et al. (2017) examined the influence of corrugations on the crashworthiness behavior of corrugated tapered tubes. They have found that the corrugations with longer wavelength yield smaller PCL during the crushing. Arnold and Altenhof (2004) examined the crashworthiness of the tubes with circular discontinuities and showed that an increase in hole diameter may lead to a decrease in PCL. However, they have noticed that the holes with very big diameters, larger than 32 mm, may induce cracks on the tubes walls during the axial crushing. Bodlani et al. (2009a, 2009b) also performed similar investigation on the crashworthiness of tubes with circular holes under axial loading. Their work also proved that introducing holes to the side walls of the tube can decrease PCL. Nonetheless, PCL was not reasonably reduced when the number of the holes was greater than two. Marzbanrad et al. (2009) studied the crashworthiness performance of a circular tube with rectangular holes on its walls. They have also reported that the holes have caused a reduction in PCL during impact.

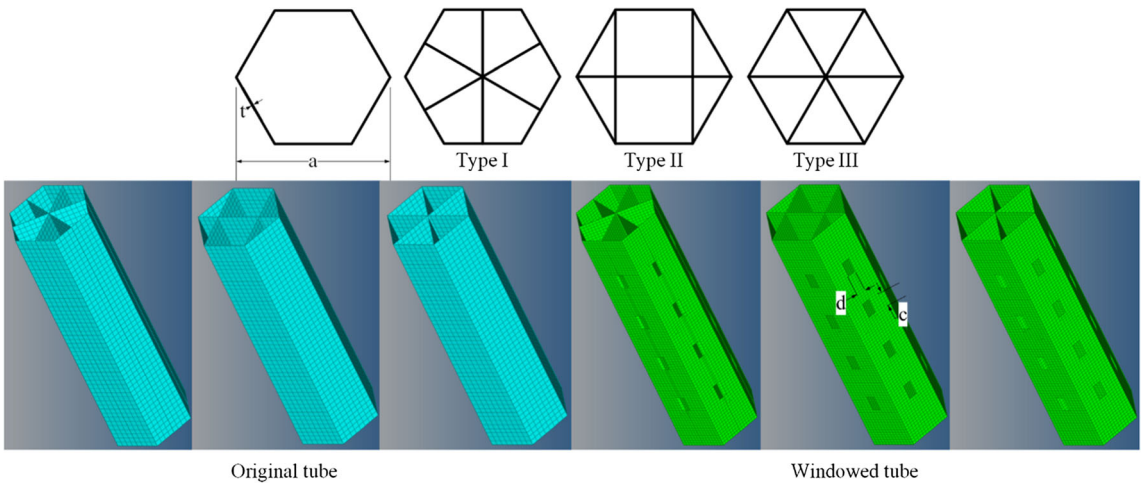

Fig. 1 Cross-sectional geometry and outlines of tubes

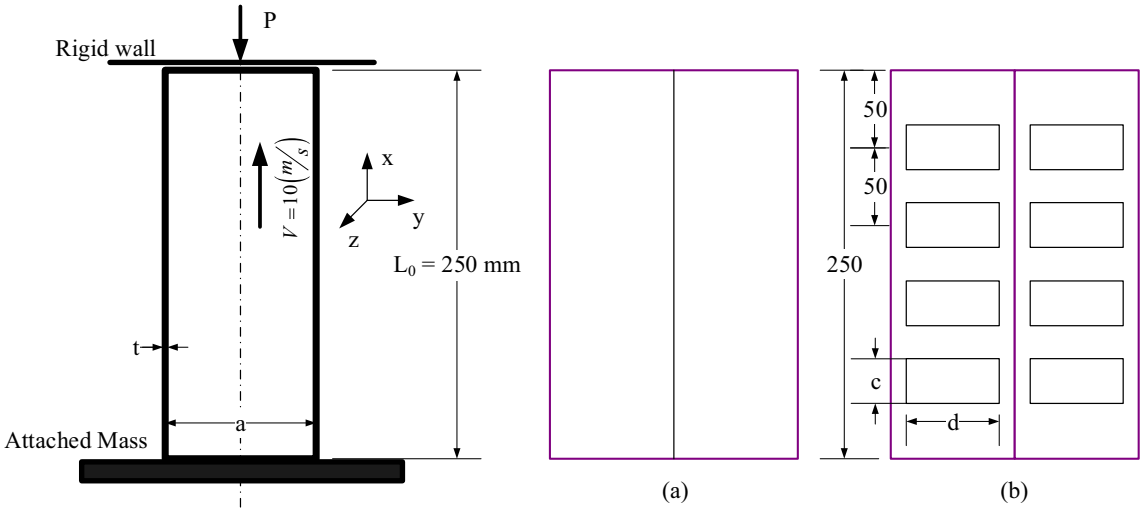

Fig. 2 Dynamic model setup: **a** STs and **b** WTs

Generally, the crashworthiness performance of a structure is influenced by different factors including its geometrical parameters and material characteristics. Design of experiments, meta-modeling, and optimization tools were employed widely for various types of structures to find the optimal crashworthiness configuration. Pareto front, which is a set of optimal solutions, is normally obtained as a result of applying the optimization process. Hou et al. (2007, 2008, 2014) used the aforementioned tools to solve a multi-objective crashworthiness optimization problem of multi-cell tubes. Tran and Baroutaji (2018) performed crashworthiness optimization analysis of multi-cell triangular tubes and analyzed their energy absorption characteristics. Yang et al. (2018) carried out design optimization of multi-cell tubes with folded patterns and evaluated the impact of the design parameters on the crashworthiness behavior. Bigdeli and Nouri (2019) combined DoE and multiple objective particle swarm optimization (MOPSO) algorism to perform the optimization of multi-cell tubes and proposed novel cross-section to improve crashworthiness performance. Other studies on the crashworthiness optimization of multi-cell tubes were also executed by Shen et al. (2017), Chen et al. (2018), Zhang et al. (2018), Luo and Fan (2018), and Yin et al. (2014, 2015, 2017).

As a summary, the aforementioned studies showed that the multi-cell structures have better crashworthiness performance than the standard single-cell ones. Also, it was widely reported that using the crush initiators on tube's wall can reduce its PCL and control its deformation behavior. However, no attempt was made in the literature to use windows crush initiators as a mean to reduce the high PCL of the multi-cell tubes. The high PCL of the multi-cell structures was considered as a limiting factor for using such structures in real-life applications (Baroutaji et al. 2017; Tran et al. 2019; Nikkhah et al. 2020). Thus, the current paper proposes new windowed hexagonal multi-cell structures and seeks their crashworthiness optimal design under axial impact loading. First, crush simulations of multi-cell hexagonal tubes without and with windows are built using LS-DYNA. Then, a two-stage optimization scheme, with SEA and PCL as objective functions, is executed to find the optimal crashworthiness design of the standard and windowed tubes. In the first step of the optimization procedure, the optimal configurations of the standard multi-cell hexagonal tubes are determined. In the second step, windows were implemented on the optimal configuration of the standard tubes, and their sizes were optimized to obtain the best windowed tubes. DoE, response surface method (RSM), and MOPSO are combined to solve the crashworthiness multi-objective optimization problem. Also, the influence of the geometrical parameters of the tube and windows on the crashworthiness behavior and collapsing modes is presented and discussed.

2 Numerical modeling

2.1 Geometry and material

Figure 1 shows the different standard and windowed multi-cell hexagonal tubes, abbreviated as STs and WTs, respectively, investigated in this paper. The circumcircle diameter, the wall thickness, and the length of the hexagonal tubes are denoted as a, t, and L_0, respectively. For WTs, rectangular windows with depth c and width d were applied to the sidewalls of the hexagonal tubes, and they were distributed equally along the tube's length. A length of 250 mm was used for all STs and WTs. Three different multi-cell configurations, as shown in Fig. 1, were created. The distinguishing feature among the three configurations is the way in which the corners and walls of the hexagonal tube are connected together to form the multi-cell geometry. Wall-to-wall (WTW) connecting webs

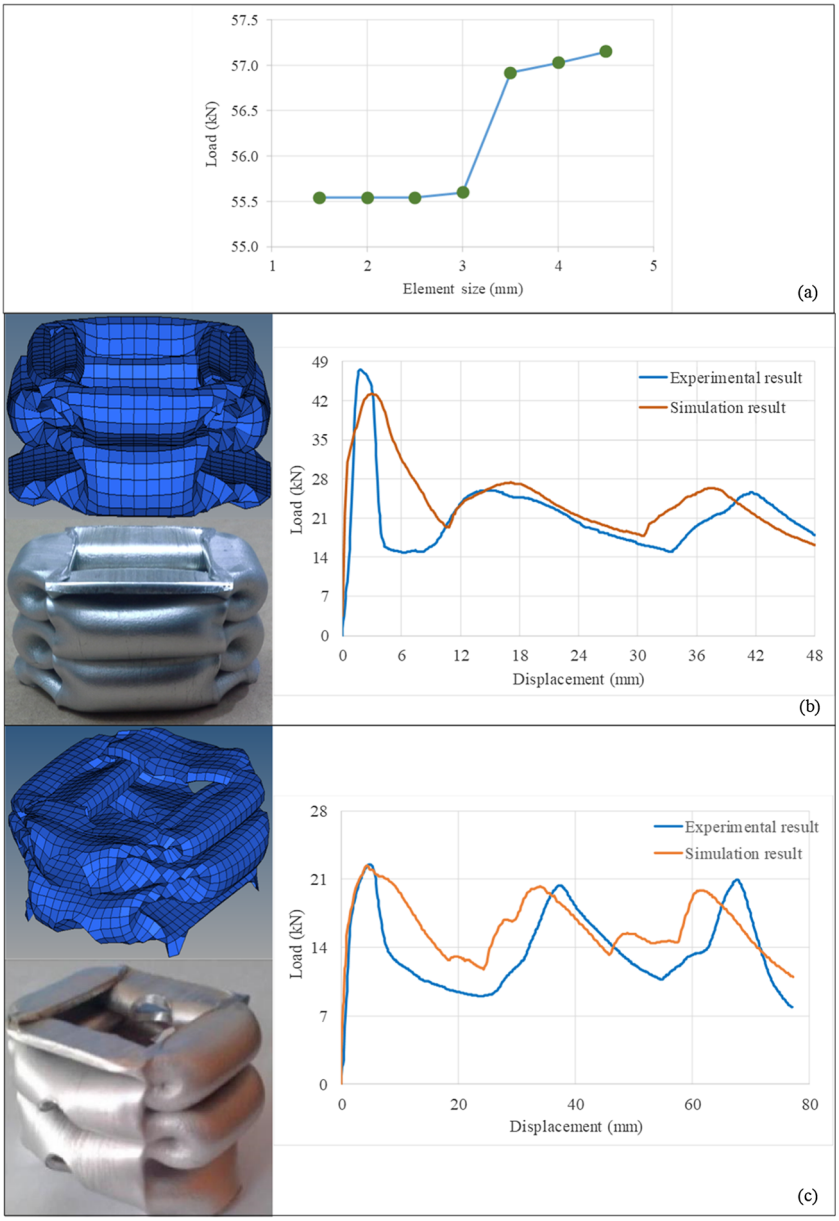

Fig. 3 **a** Convergence of load versus mesh density for tube, **b** comparison of experimental and numerical crush responses of standard square tube, and **c** comparison of experimental and numerical crush responses of windowed square tube

were used in type I, while corner-to-corner (CTC) webs were employed in types II and III. The three multi-cell types have the same values of d, L_0, and t, but they are different in weight. Tube III is the heaviest one, while tube I is the lightest. All the tubes were subjected to axial impact loading. The crush test set-up is shown in Fig. 2.

Table 1 Upper and lower levels of the design variables

Design variable	Lower level	Upper level
a	80 mm	100 mm
t	1 mm	2 mm
c	4 mm	16 mm
d	8 mm	32 mm

The tubes were made of AA6060-T4 aluminum alloy with Young's modulus of E = 68,200 MPa, initial yield stress of σ_y = 80 MPa, ultimate stress of σ_u = 173 MPa, Poisson's ration of υ = 0.3, and power law exponent of n = 0.23 for representing the stress-strain response in the plastic region (Santosa et al. 2000).

2.2 Finite element modeling

The finite element (FE) models of all tubes investigated in this paper are constructed using nonlinear explicit finite element code LS-DYNA. Hypermesh was used in the preprocessor stage to define the material model,

Table 2 Design matrix for STs

			ST-I		ST-II		ST-III	
n	*t* (mm)	*a* (mm)	SEA (kJ/kg)	PCL (kN)	SEA (kJ/kg)	PCL (kN)	SEA (kJ/kg)	PCL (kN)
1	1	80	23.5349	48.9556	19.5420	49.9765	19.3669	52.4536
2	1.3333	80	24.9536	65.1053	21.3248	68.1549	21.2796	69.4948
3	1.6666	80	27.6488	85.3953	22.7717	86.5631	22.9103	90.7504
4	2	80	29.2353	101.8220	24.2216	103.7870	24.3425	108.5170
5	1	86.6666	21.1471	53.8912	16.6479	54.5799	17.6871	57.3181
6	1.3333	86.6666	23.3821	75.4269	18.5823	74.2729	19.3320	79.8790
7	1.6666	86.6666	24.6454	93.2841	20.0148	95.2330	21.0983	98.4809
8	2	86.6666	27.4921	113.2439	21.7976	112.7276	22.7266	118.1293
9	1	93.3333	20.2535	56.8080	16.2581	59.0509	16.9106	62.0158
10	1.3333	93.3333	21.8448	79.2776	17.3988	81.9612	18.1805	84.7964
11	1.6666	93.3333	23.6454	102.7872	18.9573	103.1425	19.9011	108.7457
12	2	93.3333	24.5964	120.8286	20.2639	123.3511	21.4530	129.1745
13	1	100	18.7764	62.3113	14.4890	63.2179	16.0359	66.8882
14	1.3333	100	21.1354	85.6855	16.1602	87.4507	17.6443	90.9786
15	1.6666	100	22.7924	110.9628	17.7632	111.0468	19.0748	115.1969
16	2	100	23.7140	130.5420	19.0110	132.9300	20.1915	138.0230

meshing, loading, and boundary conditions. The model consists of a stationary rigid wall and a thin-walled tube traveling at 10 m/s. An additional mass of 500 kg was attached to the moving object to provide sufficient deformation for the tube upon impacting on the rigid wall. The thin-walled tubes were meshed using the four-node quadrilateral shell elements with one integration point in the element plane and three other integration points through the thickness. Such shell element was extensively used in the literature for modeling the crush behavior of thin-walled structures as they can accurately capture the deformation modes under the impact loading. To

Table 3 Design matrix for WTs

			WT-I		WT-II		WT-III	
n	*c* (mm)	*d* (mm)	SEA (kJ/kg)	PCL (kN)	SEA (kJ/kg)	PCL (kN)	SEA (kJ/kg)	PCL (kN)
1	4	8	14.3001	73.0413	15.3906	75.7331	16.1595	75.7108
2	8	8	13.2360	73.0103	14.9525	75.6584	15.7186	75.6907
3	12	8	12.4902	72.9713	14.8052	75.6256	15.8322	75.6567
4	16	8	12.0469	72.9056	14.6444	75.5705	16.0894	75.6085
5	4	16	13.2029	73.0239	14.1650	75.666	16.0669	75.6974
6	8	16	12.7421	72.9684	14.1173	75.464	15.4392	75.6574
7	12	16	11.7515	72.8840	14.1761	75.533	15.2700	75.5672
8	16	16	11.6389	72.5394	14.0852	75.375	15.4578	75.3691
9	4	24	13.3663	73.0188	14.7502	75.650	15.2431	75.6837
10	8	24	11.3974	72.9016	14.5461	75.577	14.9019	75.6511
11	12	24	11.9360	72.7652	14.8690	75.408	14.9217	75.4348
12	16	24	11.3879	72.1972	14.5797	74.974	14.3327	75.0167
13	4	32	13.5793	72.9805	14.2376	75.691	14.4034	75.6649
14	8	32	13.3259	72.9026	13.9893	75.528	14.6805	75.5586
15	12	32	12.4766	72.5549	14.3478	75.235	14.7812	75.2408
16	16	32	11.0900	71.9953	14.0454	74.592	14.2296	74.5733

Table 4 Summary of ANOVA analysis for STs and WTs

Tube	Model	*F* value	*p* value	Statistical measurements			
				R^2	Adj-R^2	Pre-R^2	Adeq precision
ST1	*SEA = f(a, t)*	136.82	< 0.0001	0.98	0.97	0.95	40.18
	PCL = f(a, t)	2181.26	< 0.0001	0.99	0.99	0.99	137.86
ST2	*SEA = f(a, t)*	190.54	< 0.0001	0.98	0.98	0.97	47
	PCL = f(a, t)	9765.75	< 0.0001	0.99	0.99	0.99	305.58
ST3	*SEA = f(a, t)*	897.41	< 0.0001	0.99	0.99	0.99	101.347
	PCL = f(a, t)	3840.96	< 0.0001	0.99	0.99	0.99	183
WT1	*SEA = f(c, d)*	12.76	0.0002	0.86	0.79	0.7	11.5
	PCL = f(c, d)	64.07	< 0.0001	0.96	0.95	0.89	26.25
WT2	*SEA = f(c, d)*	24.61	0.00015	0.97	0.93	0.81	16.74
	PCL = f(c, d)	28.98	< 0.0001	0.93	0.9	0.79	17.61
WT3	*SEA = f(c, d)*	51	< 0.0001	0.98	0.96	0.87	21.59
	PCL = f(c, d)	59.44	< 0.0001	0.96	0.95	0.86	25.45

decrease the impact of mesh size on the accuracy of the model's results, a mesh convergence test is performed. The mesh convergence results are presented in Fig. 3a which shows the variation of peak collapse load (PCL) of the tube with seven different mesh sizes. As it can be seen, the difference in load's value becomes very insignificant when the mesh size is less than 2.5 mm. Thus, it can be stated that an element size of 2.5 mm is sufficient to provide accurate numerical results within reasonable solution time and for this it was selected for the

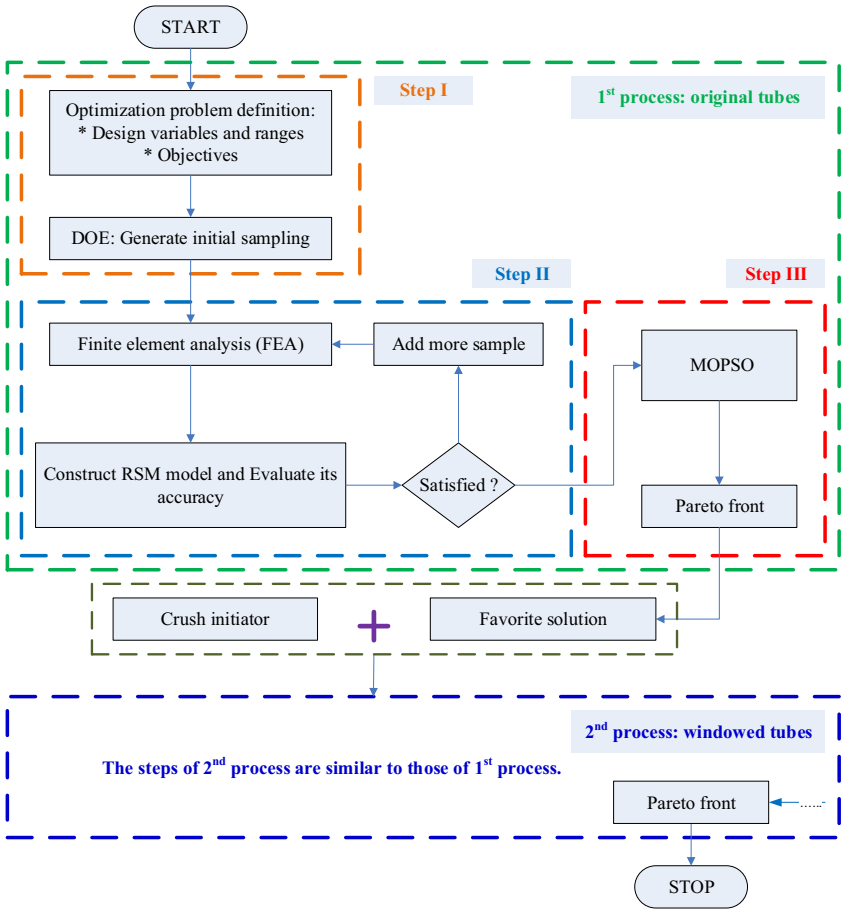

Fig. 4 Flowchart of multi-objective optimization

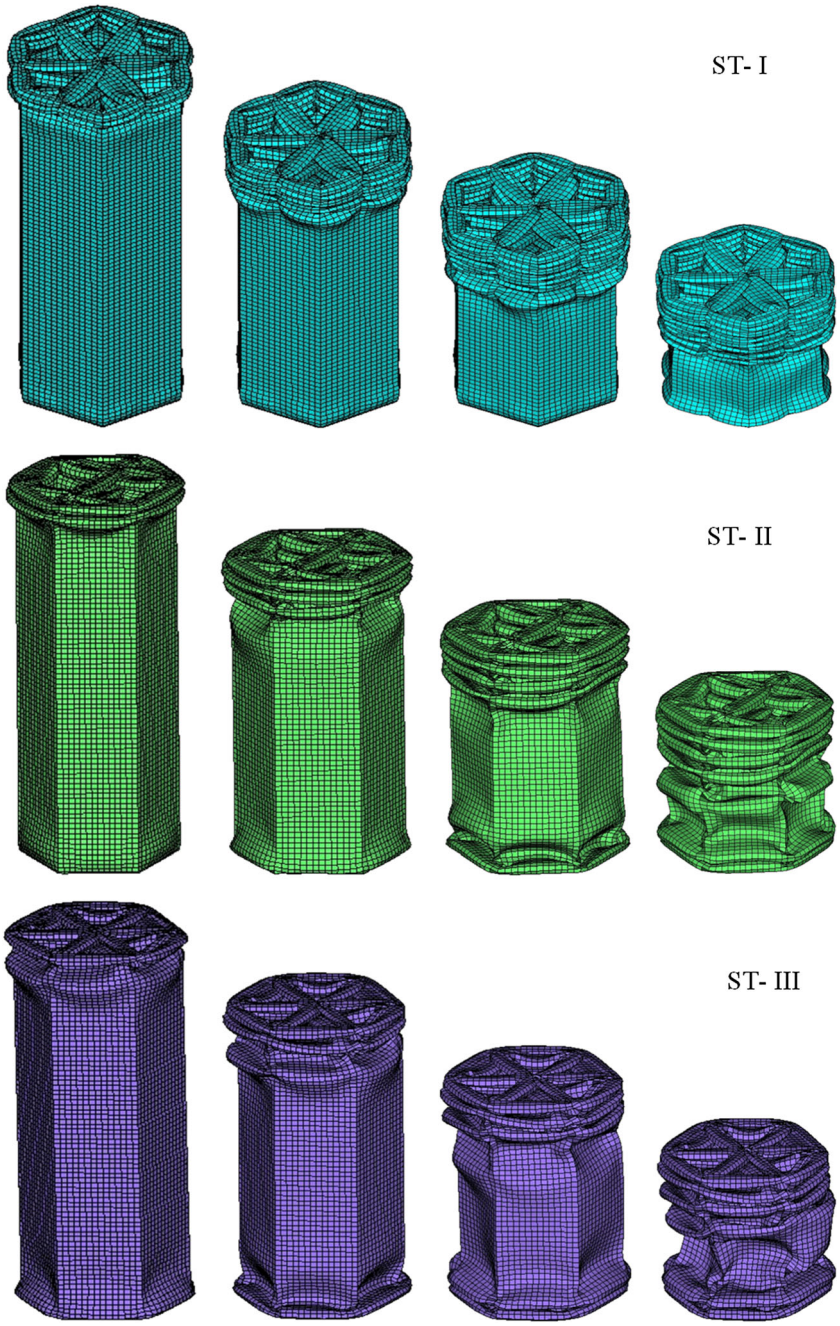

Fig. 5 Deformation history of STs

simulation. The attached mass and the rigid wall were set as rigid bodies (*MAT_20). The piecewise linear plastic material model (*MAT_24) was adopted to represent the mechanical behavior of AA6060-T4 aluminum alloy. It is evident from previous researches that AA6060-T4 is insensitive to strain rate and for this the strain rate effects were not considered in the current FE model (Santosa et al. 2000). Surface-to-surface contact with static and dynamic friction coefficients of 0.3 is employed to model the interactions between the tube and rigid walls. The self-contact experienced by the tube during the deformation was modeled using the single_surface_contact.

2.3 FE model validation

The developed FE model was first validated using a closed-form formula that was extracted by Yin et al. (2020) based on the super folding element method, and it describes the MCL of ST-III multi-cell hexagonal tube as function of tube's thickness (t) and circumcircle diameter (a) as given in (1).

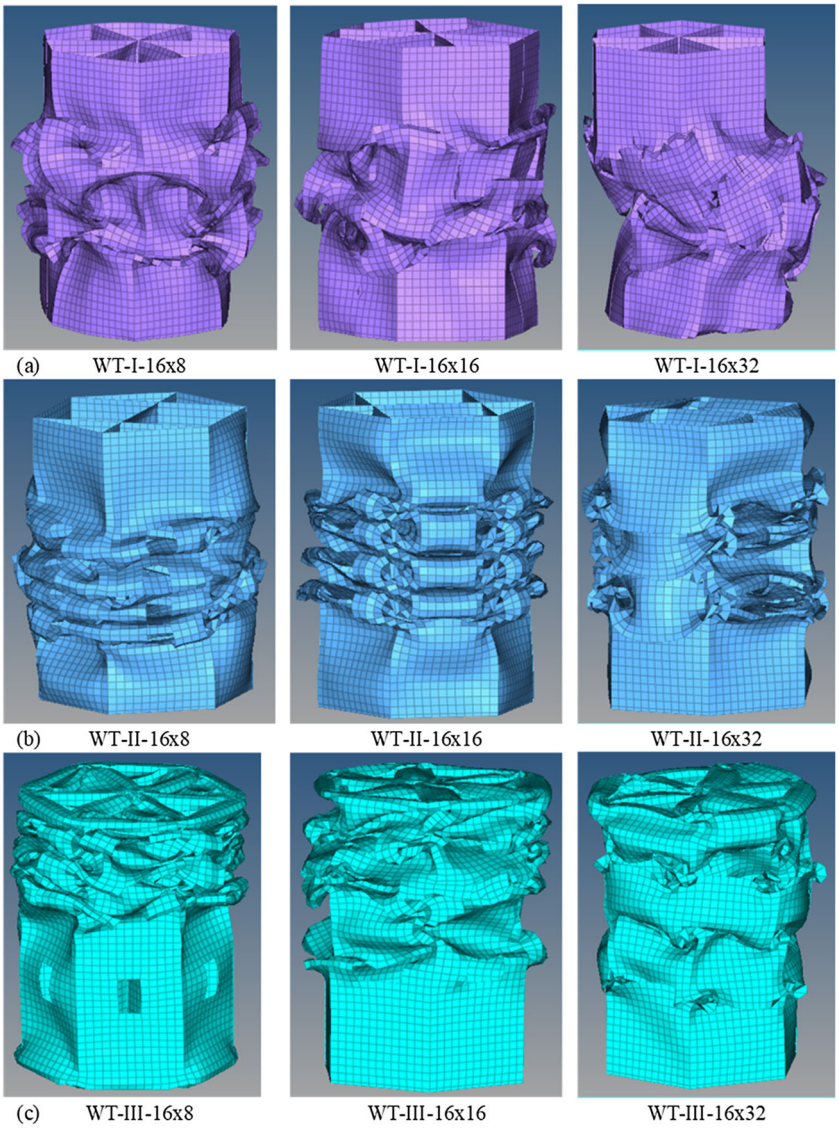

Fig. 6 Deformation history of WTs: **a**) WT-I, **b**) WT-II, and **c**) WT-III

$$MCL = \gamma \frac{6}{2k} \sigma_o t^{1.5} (a/2)^{0.5} \sqrt{2\pi\left(1 + 2\cos\left(\frac{\pi}{2} - \frac{\pi}{6}\right)\right)\left(1 + 2\tan\left(\frac{\pi}{4} - \frac{\pi}{12}\right) + \tan\left(\frac{\pi}{2} - \frac{\pi}{6}\right)\right)} \quad (1)$$

where σ_o is the material's flow stress, γ is the dynamic enhancement factor and was set as 1.1, and k is the crushing distance coefficient and was set as 0.75.

Based on the above equation, the MCL for ST-III was calculated as 58.3 kN when D and t were selected as 80 mm and 2 mm, respectively. The average force obtained using the FE simulation was 62 kN. By comparing the analytical and the simulated MCL, it can be seen that the FE model can predict the MCL with only 6.5% relative error.

To further validate the material model used in the finite element model developed in this paper, experimental test data reported by Nikkhah et al. (2019) on the crushing of simple and windowed square tubes made of AA6060-T4 was adopted. Crush simulations of the square tubes were also executed in LS-DYNA with the same boundary conditions as those used in the experiments. A comparison of the numerical and experimental results is presented in Fig. 3b and Fig. 3c. As it can be seen from the crushing response, the numerical crushing forces are slightly lower than the experimental ones, particularly for the windowed tubes, which might be due to the inability of the FE model to accurately capture the inhomogeneous axial stiffness of the tube caused by the material cutaway in the windows' zone. However,

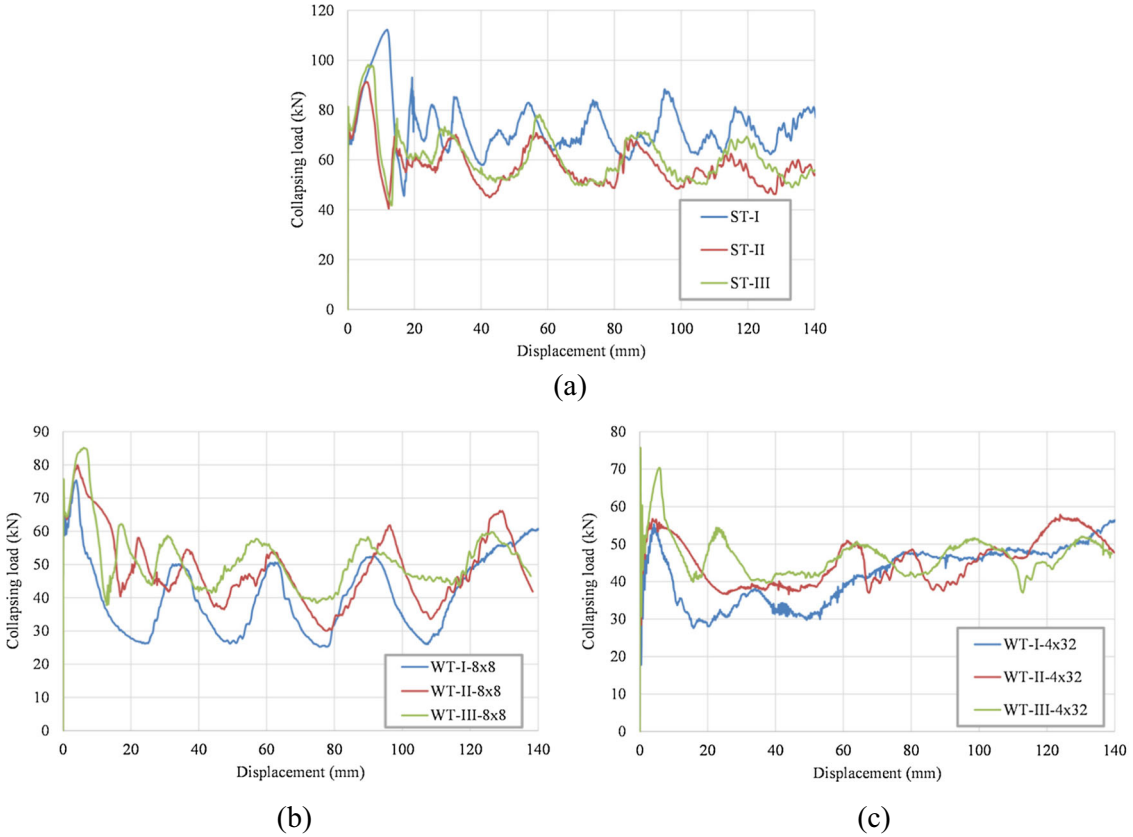

Fig. 7 Force-displacement responses of **a** STs with $a = 93.3333$ mm and $t = 1.3333$ mm, **b** WTs with windows' size of 8×8 mm, and **c** WTs with windows' size of 4×32 mm

the experimental and simulation results in terms of the collapsed configuration and load-displacement responses are still in a satisfactory agreement. Thus, it can be considered that the developed FE model is sufficiently accurate and can be used to simulate the responses of STs and WTs tubes under axial impact.

3 Crashworthiness optimization designs

3.1 Crashworthiness metrics

The crashworthiness performance of STs and WTs is appraised via different crashworthiness indices, such as energy

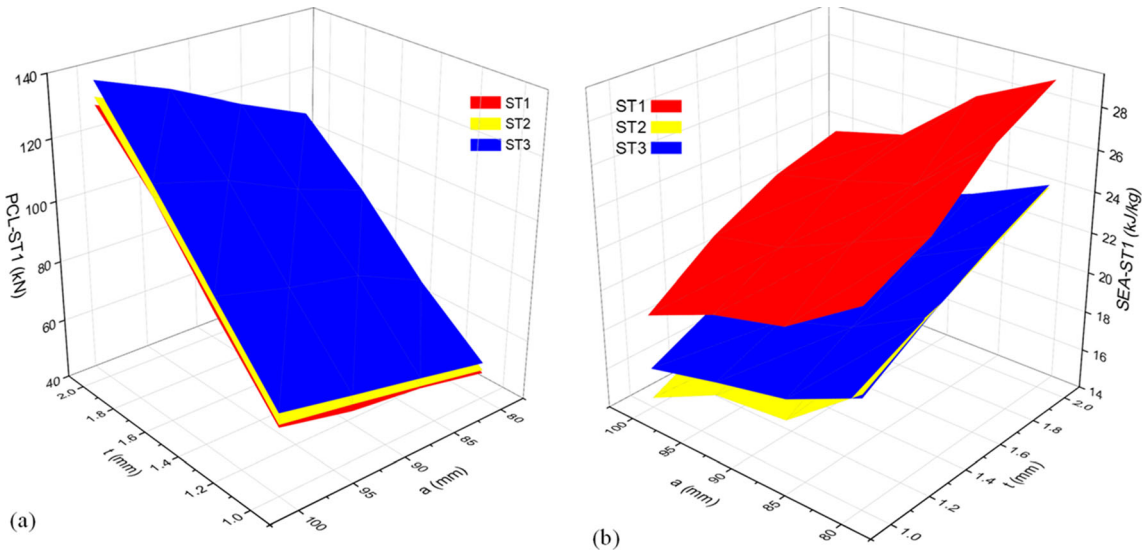

Fig. 8 Variation of **a** PCL and **b** SEA with geometrical parameters of STs

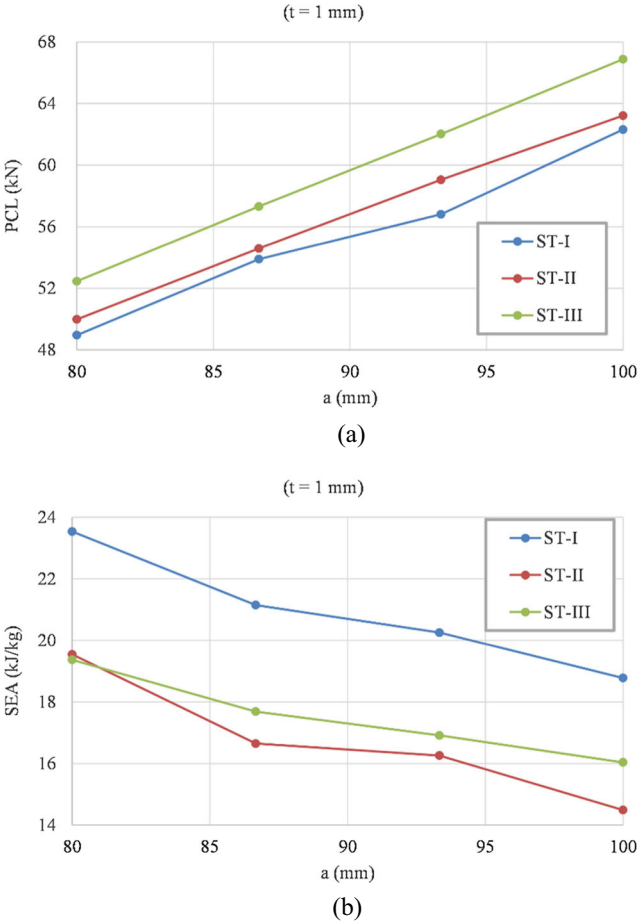

Fig. 9 Effects of a on **a**) PCL and **b**) SEA of STs

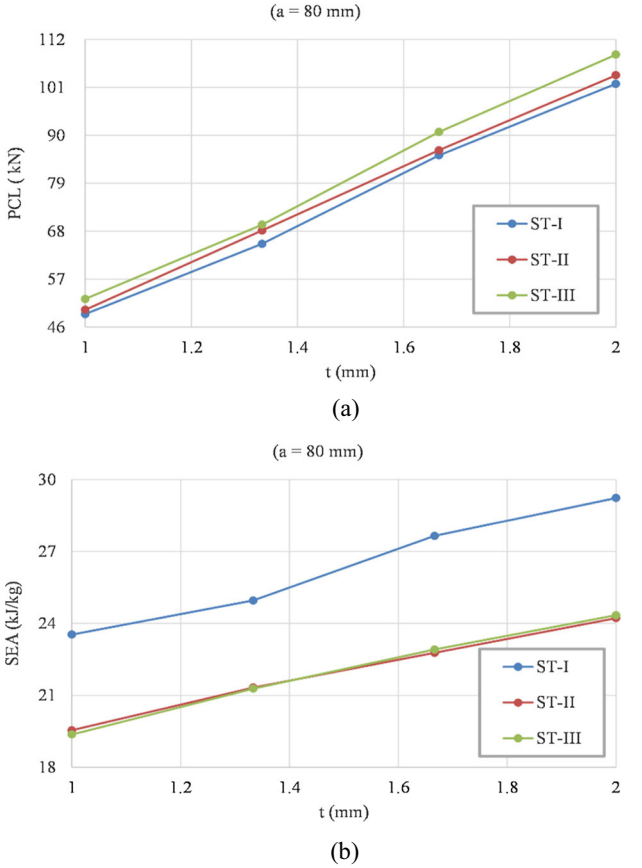

Fig. 10 Effects of t on **a**) PCL and **b**) SEA of STs

absorption capacity (E_A), PCL, SEA, and mean collapsing load (MCL), which are deliberated previously in the literature and extensively utilized for evaluating the crush and energy absorption behaviors of thin-walled tubes (Sun et al. 2011, 2014, 2017).

The energy absorption capacity or the energy absorbed by tube (E_A) is the strain energy absorbed during the collapsing process, and it is normally given as shown in (2)

$$E_A = \int_0^{\delta} P(u)du \tag{2}$$

where $P(u)$ is the instantaneous collapsing load as a function of collapsing distance and δ is the total collapsing distance.

Specific energy absorption (SEA) is a key index representing the amount of energy that can be absorbed per unit mass of a structure; SEA can be calculated as demonstrated in (3)

$$SEA = \frac{E_A}{m} \tag{3}$$

where m is the mass of the tube.

PCL is the maximum value of $P(u)$ which corresponds to peak deceleration. Considering the vehicle impact, a high PCL often leads to a large damage and severe injury or death of the vehicle's occupants. The PCL of an absorber should therefore be reduced and constrained to the survivable levels.

Collapsing load efficiency (CLE) is another valuable dimensionless crashworthiness indicator which can be defined as the ratio between the mean collapse load (MCL) and the PCL, as shown in (4)

$$\text{CLE} = \frac{\text{MCL}}{\text{PCL}} \tag{4}$$

MCL can be obtained using (5)

$$MCL = \frac{E_A}{\delta} \tag{5}$$

3.2 Design of experiment

The first step of establishing the meta-model of the crashworthiness metrics is to choose a sampling technique to generate the design points. Sampling strategy is very crucial for balancing the accuracy of the meta-models and the number of runs required therefore an effective sampling technique

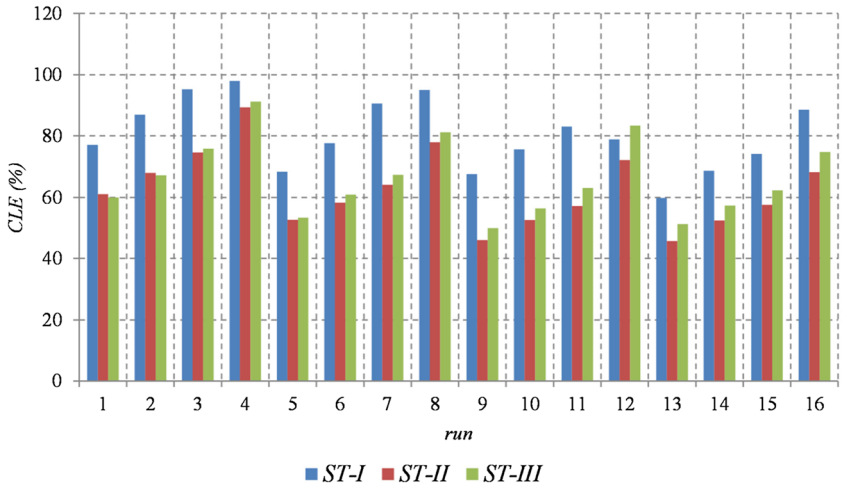

Fig. 11 CLE response of all STs at the design points

should be used. Design of experiment (DoE) approach is usually applied to build an effective mesh of training points within the design space (Hou et al. 2011, 2012, 2013; Baroutaji et al. 2014, 2015; Acar et al. 2011). The main sampling techniques offered by DoE are Latin hypercube sampling, orthogonal design, and full factorial design (FFD). Taking the benefits of furnishing the design region with uniformly distributed sampling points, FFD is adopted in this study to create the design points. The geometrical parameters of the tubes and the windows, namely, a, t, c, and d, as presented in Section 2.1, were selected as design variables. The upper and lower levels of these design variables are presented in Table 1. Applying the FFD on the four design variables has resulted in total 16 design points within the design space.

3.3 Response surface method

After generating the design points, axial crush simulations of the different STs and WTs were conducted at the design points using LS-DYNA, and the SEA and PCL values were calculated. The design variables, i.e., a, t, c, and d, and the design responses, i.e., SEA and PCL, as obtained from the numerical simulations are presented in Tables 2 and 3 for STs and WTs, respectively. Following obtaining the SEA and PCL values at the training points, response surface method (RSM) was then adopted to construct the meta-models of SEA and PCL responses required for crashworthiness optimization and parametric analysis. The aforementioned crashworthiness metrics, i.e., SEA and PCL, were calculated up to a crushing distance of 140 mm in order to avoid any undesirable crush behavior at high displacement, thus providing more realistic crashworthiness analysis within the practical crush zone. The RSM demonstrated good approximation accuracy for highly nonlinear crashworthiness optimization problem, and it was adopted extensively in previous researchers (Hou et al. 2007, 2008, 2009; Nguyen et al. 2016, 2017).

After building the meta-models, they should be tested for accuracy to ensure their validity for the analysis. Hence, the analysis of variance (ANOVA), which provides detailed

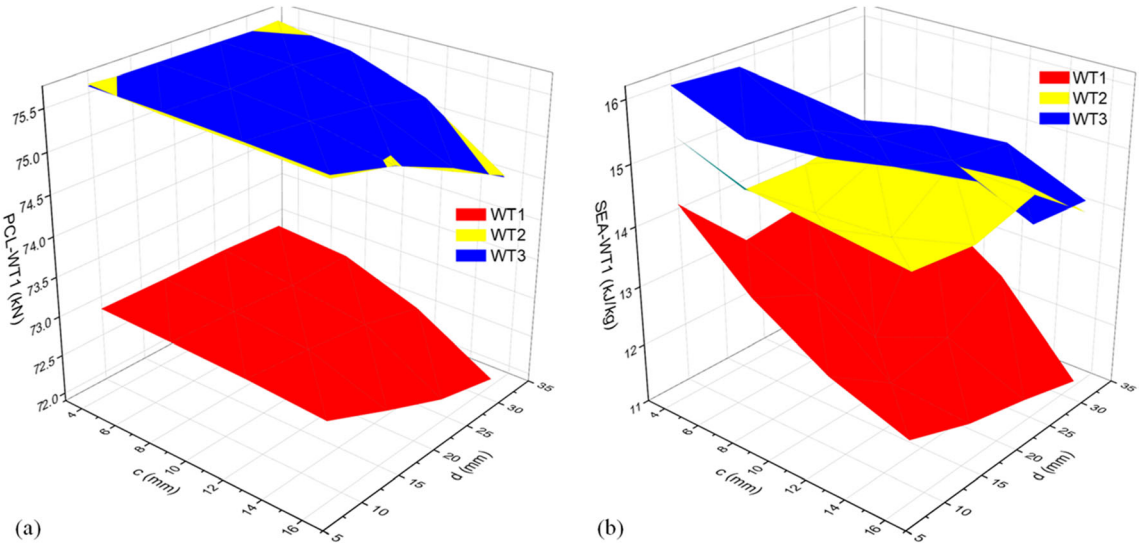

Fig. 12 Variation of **a** PCL and **b** SEA with the geometrical parameters of WTs

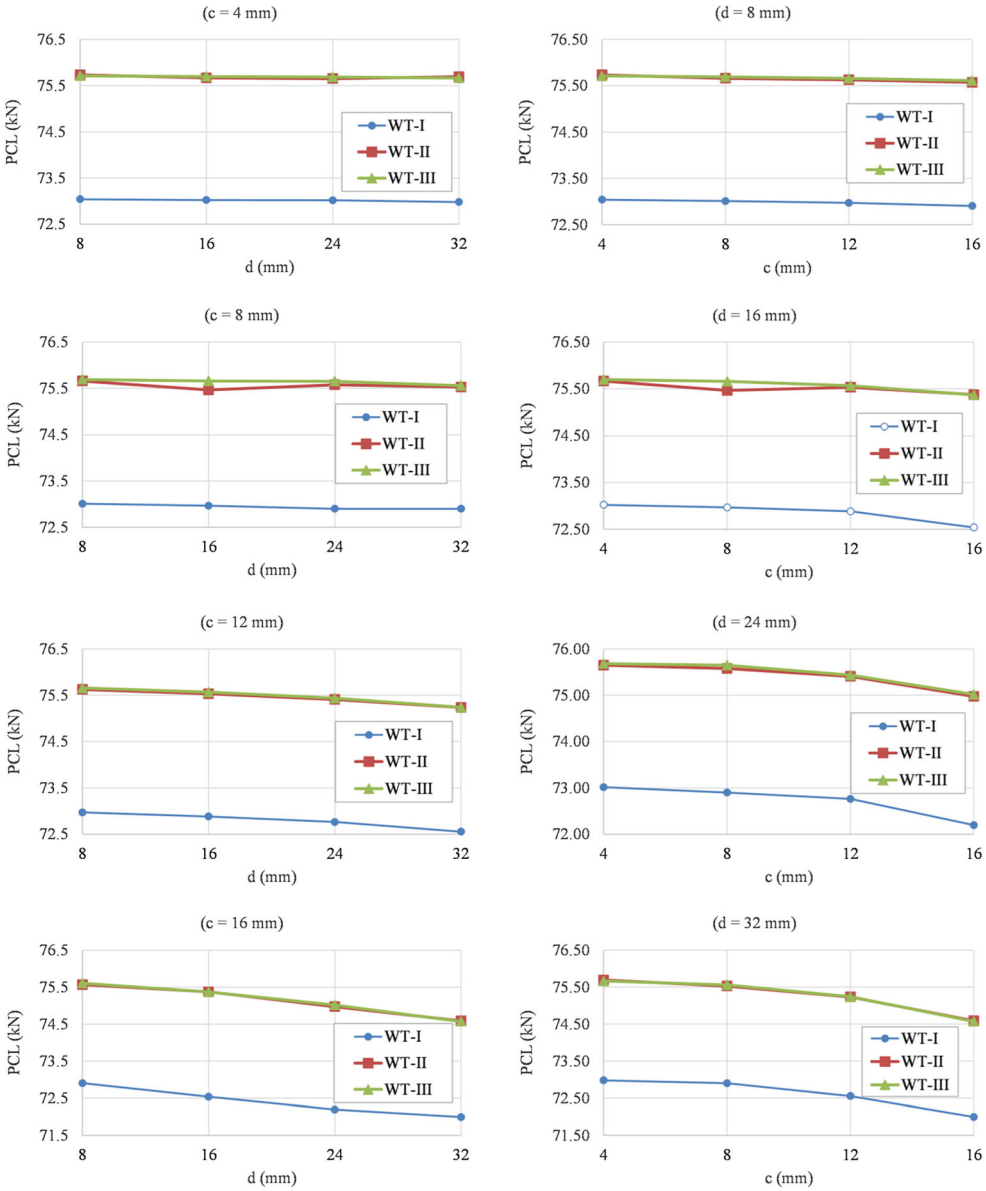

Fig. 13 Effects of c and d on PCLs of all WTs

information about the model statistical significance measures, such as coefficient of determination (R^2), adjusted coefficient of determination (Adj-R^2), and Adeq precision, was used to check the adequacy of the developed meta-models for SEA and PCL. Table 4 shows a summary of ANOVA analysis for STs and WTs, for which the statistical measures are listed. As it can be seen, all meta-models exhibit high F values and small p values. The F values, ranging from 12.76 to 3840.96, point out that these models are significant. The small p values confirm that there is very small opportunity that the F value could occur due to noise. Additionally, the R^2, of all meta-models, ranges from 0.86 to 0.99 indicating that the meta-models provide an excellent fitting of the data points. The values of Pre-R^2, ranging from 0.7 to 0.99, are in very good agreement with the Adj-R^2 values. The Adeq precision, which measures the signal to noise ratio, is above 4 for all meta-models indicating excellent adequacy for them.

3.4 Formulation of optimization problem

One of the problematics in design optimization for vehicle crashworthiness is the selection of appropriate objective functions. Different combinations of the various crush responses such as EA, peak acceleration (PA), PCL, and SEA tend to be employed as objective functions in the crashworthiness optimization problems. When maximizing SEA is considered to be one objective, it should be accompanied by restraints on PCL to ensure the safety performance of the vehicle. Contrary to the single-objective optimization which offers only one optimal solution, the multi-objective optimization provides a set of optimal solutions, which permits larger design range for designers. For the current study, PCL and SEA are selected as the objective functions to be minimized and maximized, respectively. The geometrical parameters of tubes and windows including a, t, c, and d

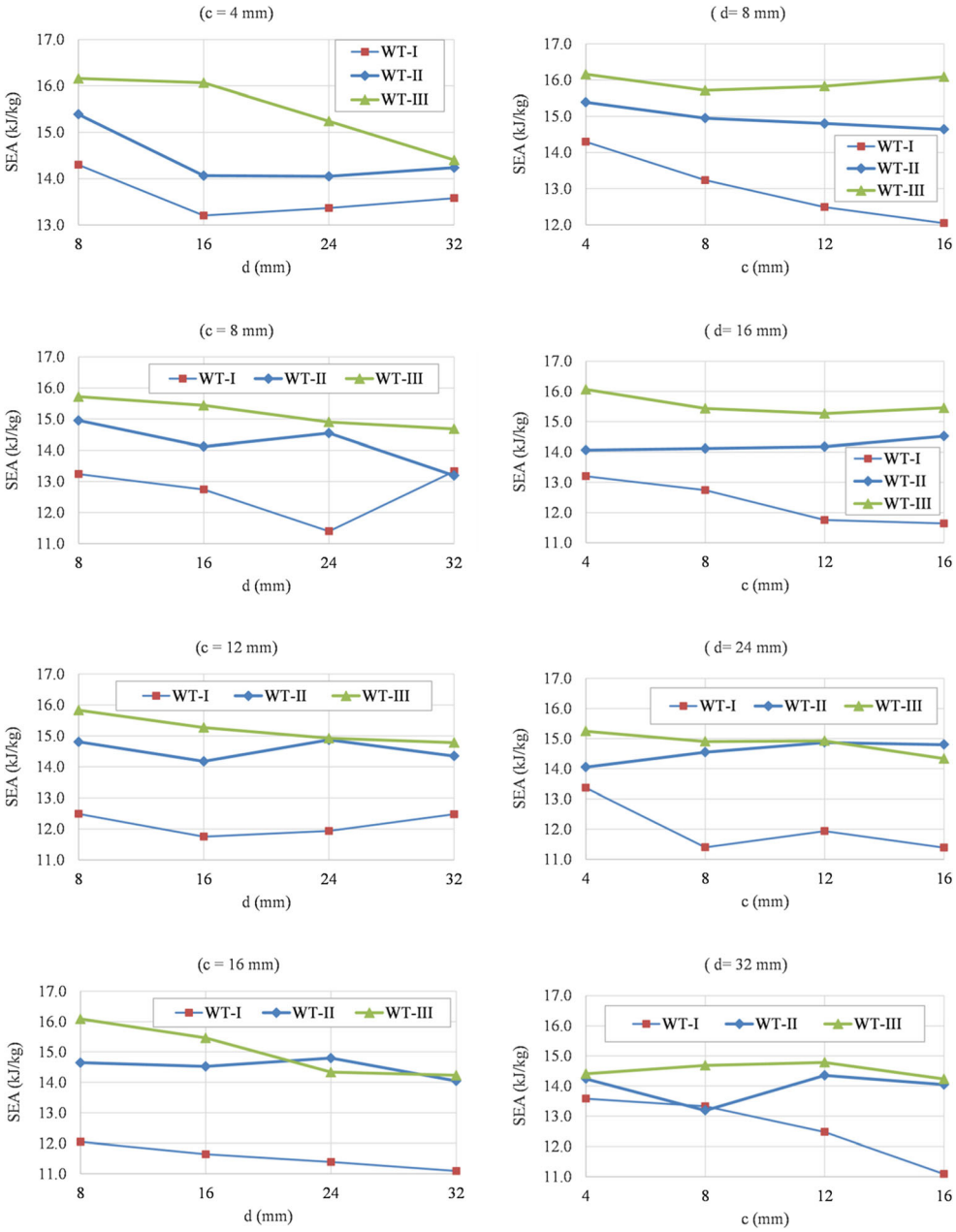

Fig. 14 Effects of c and d on SEAs of all WTs

were set to vary within their limits. The optimization problem of STs and WTs can be formulated as shown in (6)

$$\left|\begin{array}{l} 1^{st}\,\text{process}(STs): \begin{cases} \begin{bmatrix}\text{Maximize} & SEA\\ \text{Minimize} & PCL\end{bmatrix} \\ s.t \quad 80mm \le a \le 100mm \\ \qquad\quad 1mm \le t \le 2mm \end{cases} \\ 2^{nd}\,\text{process}(WTs): \begin{cases} \begin{bmatrix}\text{Maximize} & SEA\\ \text{Minimize} & PCL\end{bmatrix} \\ s.t \quad 4mm \le c \le 16mm \\ \qquad\quad 8mm \le d \le 32mm \end{cases} \end{array}\right. \tag{6}$$

3.5 Multi-objective optimization procedure

Optimization algorithms are required to solve the multi-objective optimization problem presented in (6) and to perform the trade-off between the two conflicting design objectives and to generate a series of optimal solutions known as the Pareto front. Among the most common optimization algorithms such as Multi-Island Genetic Algorithm (MIGA), Non-dominated Sorting Genetic Algorithm (NSGA), and Multi-Objective Particle Swarm Optimization (MOPSO), MOPSO is characterized by the fast convergence and well-distributed Pareto front, and it was selected for finding the Pareto fronts of the different STs and WTs. A flowchart

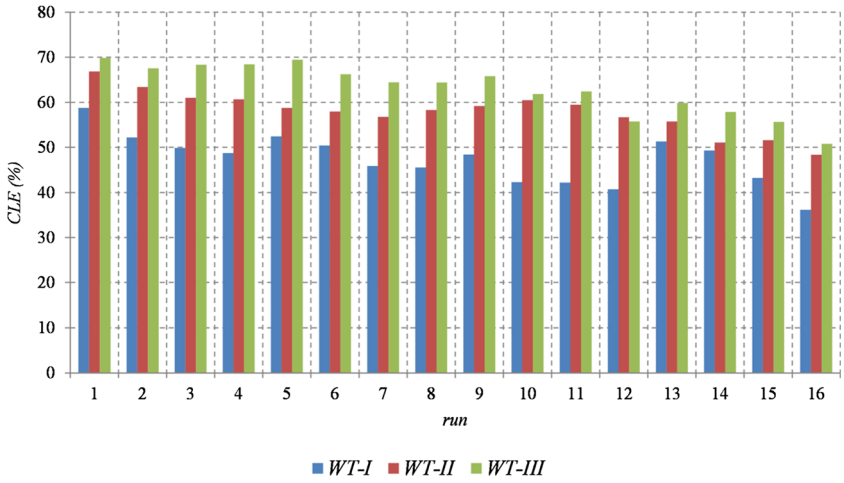

Fig. 15 CLE response of all WTs at the design points

illustrating the multi-objective optimization process of STs and WTs is introduced in Fig. 4.

The optimization procedure contains two processes with identical steps. Each optimization process has three main steps. The first step is to define the crashworthiness optimization problem for STs and to select the design variables and design space. In the second step, crush simulations using FE models are carried out to get the crashworthiness indicators at the sampling points and then construct the meta-model of the crush responses using RSM. In the last step, the MOPSO solves the crashworthiness optimization problem, and the Pareto fronts, i.e., a series of optimal solutions, of the STs are obtained. A favorite optimal solution for each type of STs is chosen from its corresponding Pareto front based on specific design requirements using the minimum distance selection method. Following that, the obtained optimal design of each ST is combined with windows to build WTs, and then the second optimization process is executed to get the Pareto fronts for each WT.

4 Results and discussion

4.1 Deformation modes and crush responses of STs and WTs

In order to analyze the crushing behavior of STs, their deformation processes of STs with $a = 93.3333$ mm and $t = 1.3333$ mm are laid out in Fig. 5. The crashworthiness metrics and the crush responses were calculated up to a displacement of 140 mm in order to avoid the extreme increase in the crush force at the end of the deformation process caused by the crumpling of the tube's material. The selected crush distance, i.e., 140 mm, allows for more sensible estimation of the crashworthiness behavior of the investigated tubes. Although all STs deform in a progressive folding way, they reveal different folding aspects. The CTC and WTW connection webs play an important role in determining the deformation mode of the standard multi-cell tubes. The deformation mode of ST-I with WTW connection webs is more regular with shorter wavelength and greater number of folds than those observed for ST-II and ST-III. This could be due to the fact that the WTW webs may have improved the lateral stiffness of the sidewalls of ST-I leading to more stable and better deformation mechanism. The CTC webs in ST-II and ST-III do not seem to enhance the lateral stiffness of the tubes, and therefore, their deformation mechanisms involve lower number of folds with greater wavelength than those of ST-I. So in summary, it can be reported that ST-I has more favorable progressive collapsing mode than the other standard tubes. Such folding mode is desirable as it can improve the energy absorption capacity of the structure.

To analyze the effects of implementing windows on the sidewalls of the STs, the final deformation patterns of WTs with various windows' sizes are illustrated in Fig. 6. It is clear that all WTs deform in a progressive folding fashion. The wrinkling of the WT-I and WT-II occur at their middle regions while WT-III wrinkles at its upper part. Generally, as it has been previously reported in the literature, by introducing windows into a tube, its folding mode can be efficiently controlled, and the global buckling can be prevented, and this appears to be the case for WT-II and WT-III. However, the WT-I with larger windows' size seems to undergo some sort of global bending which negatively affects its crashworthiness characteristics. Generally, the plastic deformation is initiated in the zones possessing lower stiffness due to its relatively low ability to support load, and then it continuously progresses to zones with higher stiffness during the crushing process. Based on this feature, the desired collapse mode of the WTs can be achieved by controlling the locations of the windows. Comparing the failure modes of all WTs, it seems that the WT-II has the most regular and stable failure mode with the higher number of folds. When increasing the window's size, the global buckling phenomenon appears in WT-I, while the

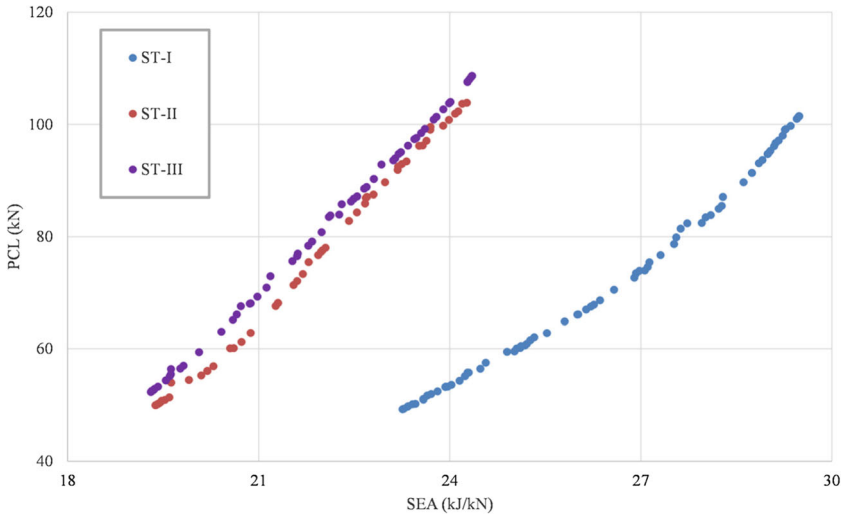

Fig. 16 Pareto fronts for STs

deformations of WT-II and WT-III remain progressive and stable. For WT-I, the larger the windows are, the more unstable the deformation mode is.

The load-displacement curves of STs and WTs are plotted in Fig. 7. The load histories of tubes during crushing are valuable data to estimate the overall collapsing performance. It is clear that the different tubes offer similar force-displacement responses. After the first loading peak, the collapsing load fluctuates several times to form wrinkles during the crushing process. For STs, the level of collapsing load of ST-I is greater than those of ST-II and ST-III indicating a higher MCL index. However, for WTs, the levels of the crushing load of WT-II and WT-III are greater than that of WT-I. Therefore, MCLs of WT-II and WT-III are improved compared to WT-I. Figure 7 also shows that the load fluctuation of WTs with windows' sizes of 4×32 mm is smaller than those of WTs with windows' size of 8×8 mm. This can be linked with the fact that the WTs with bigger windows' size require less force to generate the successive folds during the crushing.

4.2 Parametric analysis

The geometrical shape of the energy absorption structure dominates its responses to the dynamic loading. Thus, in order to fully understand and evaluate the performance and safety of STs and WTs, the influence of their main geometrical parameters, such as a, t, c, and d, on their crashworthiness indexes is presented in this section.

4.2.1 Influence of a and t on the crashworthiness metrics of STs

Figure 8 shows surface plots depicting the variation of SEA and PCF with the geometrical parameters for all STs. It can be seen that ST-I has a slightly lower PCL and greater SEA than the other STs for all values of t and a. ST-III offers slightly higher PCL and SEA than those of ST-II. Such observations confirm that WTW connection implemented in ST-I is more

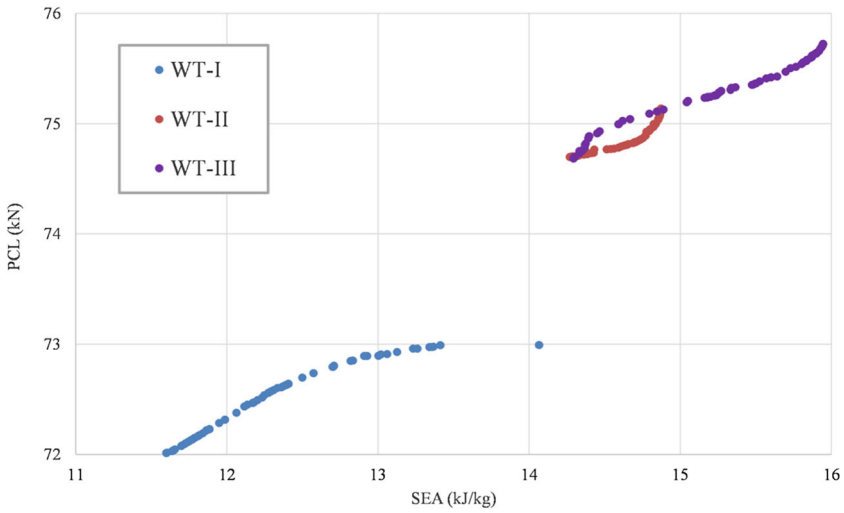

Fig. 17 Pareto fronts for WTs

Table 5 Selected optimal solution of (a) STs and (b) WTs

	Tube	a (mm)	t (mm)	PCL (kN)	SEA (kJ/kg)
(a)	ST-I	1.4526	80.4144	73.8992	26.9768
	ST-II	1.4795	80.0152	76.6951	21.9340
	ST-III	1.4175	80.0104	76.5015	21.6056
(b)	WT-I	4.0275	8.1097	72.9910	14.0661
	WT-II	15.9597	27.7413	74.8696	14.7528
	WT-III	14.8256	9.2571	75.6034	15.8717

effective for the standard tubes than the CTC connection type used in ST-II and ST-III.

Figure 9 illustrates the changes of PCL and SEA with a when $t = 1$ mm. It is clear that crashworthiness indexes of STs are considerably influenced by a. From the figure, it can be seen that by increasing a, PCL increases and SEA decreases. Under the same values of t and a, ST-I shows smaller PCL and greater SEA than those recorded in ST-II and ST-III. When a reaches to 80 mm, the SEA of ST-II falls more rapidly compared to those of ST-I and ST-III.

Figure 10 depicts the variation of SEA and PCL with t when a equals to 80 mm. It is clear that both PCL and SEA steadily rise with the increase of t. Also, it can be seen that ST-I exhibits greater SEA and smaller PCL than ST-II and ST-III for all values of t. PCLs and SEAs of ST-II and ST-III are approximately equal. When t is above 1.3333 mm, the rate of increase of SEA with t of ST-I is smaller than those of ST-II and ST-III. Although increasing t can improve the energy absorption, it also causes PCF to be substantially increased.

The values of CLE index for all STs at the 16 design points are exhibited in Fig. 11. This index is also a key crashworthiness response which gives a good idea about the collapse character and the bearing capability of the tubes. As shown in Fig. 11, it is clear that ST-I is the best performing design in terms of CLE. Figure 11 can also be used to extract the influence of t and a on CLE. It can be seen that when t increases, CLE of all STs increase.

4.2.2 Influence of c and d on the crashworthiness metrics of WTs

The variations of PCL and SEA with c and d are presented in Fig. 12 for all WTs. Comparing with STs, PCL and SEA are reduced substantially in WTs and continuously reduced with increasing windows' dimensions. PCL is directly related to the stiffness of the weakest region of the tube, and therefore, the larger windows' size means a less stiffness of the tube and thus smaller PCL is required. Contrary to the observations on STs, PCLs and SEAs of WT-II and WT-III are considerably larger than those of WT-I. WT-I exhibits slightly lower PCL than both WT-II and WT-III which can be considered an advantage for this tube. However, WT-I does not seem to perform well in terms of SEA as it absorbs less energy than WT-II and WT-III, respectively. This might be due to the undesirable interactions between the windows located on the sidewalls of WT-I and the WTW webs which are connecting its walls together. The PCL of WT-III is close to that of WT-II, but it offers higher SEA than WT-II.

The variations of PCLs of all WTs with windows' size are illustrated in Fig. 13, which shows that the PCLs of WT-II and WT-III are greater than that of WT-I for all windows' sizes. The general trend is that WTs with larger windows size yield smaller PCL. The changes in PCL are quite limited and ignorable for all WTs with small windows' sizes. The PCL changes become more observable for WTs with larger windows sizes. When $d = 32$ mm, PCLs of all WTs decrease significantly by increasing c. Interestingly, PCL shows a negligible variation with c when $d = 8$ mm. For WT-II with d of 16 mm, PCL variation with c seems to be unstable as it decreases first, then rising, before declining again.

Figure 14 shows the variations of SEAs of all WTs with the windows' parameters including c and d. Irrespective of windows' size, WT-I performs less than the other WTs in terms of SEA. Interestingly, WT-II and WT-III show very comparable SEA values for the different windows' parameters indicating that the configuration of the CTC connection webs has limited effects on SEA. SEAs of WT-I with d of 8 mm, 16 mm, and

Table 6 Verification of the chosen optimal solutions for STs and WTs

Tube	Chosen solution from Pareto front		FE simulation		Error (%)	
	PCL (kN)	SEA (kJ/kg)	PCL (kN)	SEA (kJ/kg)	PCL	SEA
ST-I	73.8992	26.9768	76.22	29.12	3.04	7.36
ST-II	76.6951	21.9340	77.4	24.18	0.91	9.29
ST-III	76.5015	21.6056	78.288	23.48	2.28	7.98
WT-I	72.9910	14.0661	76.88	15.23	5.06	7.64
WT-II	74.8696	14.7528	77.46	16.21	3.34	8.99
WT-III	75.6034	15.8717	79.98	17.14	5.47	7.40

32 mm are monotonically decreasing with increasing of c. However, for all WT-II and WT-III, the SEA curves do not show any regular pattern with respect to their changes with the windows' sizes.

The values of CLE for all WTs at the design points are introduced in Fig. 15. It can be seen that WT-III shows the highest CLE among all WTs where the WT-III with the smallest windows' size exhibits the maximum CLE response.

4.3 Optimization results

As described by the optimization flowchart in Fig. 4, the generated meta-models of SEA and PCL were used in MOPSO algorithm to solve the optimization problem of STs and WTs as presented in Eq. (6). Three Pareto fronts of PCL against SEA for STs and WTs are plotted respectively in Figs. 16 and 17, which show that PCL and SEA indexes conflict with each other and any reduction in PCL is associated with a decrease in SEA. The most satisfactory optimal design of each of STs or of WTs is then determined from the Pareto fronts using the minimum distance selection method (Branke et al. 2004; Sun et al. 2011; Tran et al. 2014) and shown in Table 5. For STs Pareto front as shown in Fig. 16, the Pareto fronts of ST-II and ST-III are located on the left side of the graph, while Pareto front of ST-I is on the right side, and this reveals that ST-I delivers higher SEA than ST-II and ST-III for the same value of PCL. This gives strong evidence that ST-I is preferable to ST-II and ST-III in terms of crashworthiness performance. Concerning the WTs and as shown in Fig. 17, the Pareto fronts of WT-II and WT-III are above and to the right of WT-I, which points out that the crashworthiness characteristics of the WT-I are inferior to those of WT-II and WT-III. STs exhibit greater SEA than WTs which is a desirable feature for real-world crashworthiness applications. Such behavior is due to the fact that the STs have more material than WTs to deform plastically and dissipate the kinetic energy. Numerical crush simulations were undertaken using the FE model to verify the chosen favorite solution. As it can be seen from Table 6, the percentage errors between the optimization and simulation values of SEA and PCF for all STs and WTs are small, and this confirms the validity of the obtained optimization results.

It is worth noting that the geometrical dimensions of the optimized WTs, i.e., a and t, were determined based on the results of the first optimization process conducted on STs as detailed in the multi-objective optimization scheme shown in Fig. 4. Thus, there might be better optimized configurations for the WTs if a different optimization scheme that simultaneously considers all the geometrical and windows parameters was adopted.

5 Conclusion

In this study, the crashworthiness optimization analysis was conducted on six different multi-cell standard and windowed hexagonal tubes. Wall-to-wall (WTW) and corner-to-corner (CTC) webs were used to create their different multi-cell configurations. A two-stage sequential optimization procedure was used to find the most suitable design for the standard configuration and then to optimize the windows' size that should be implemented on it. Validated FE model was established and used to run the crush simulations required for the crashworthiness analysis of the different designs. The influence of geometrical parameters on the crashworthiness responses of the standard and windowed tubes was determined via conducting comprehensive parametric analysis. Meta-modeling, i.e., RSM, and multiple objective optimization, i.e., MOPSO, tools were combined to find the optimal design of all examined structures. It was found that the standard design with WTW connection web performs better than all other designs and absorbs the greatest energy per unit mass. However, for the windowed tubes, the WTW webs were not effective, and the tube with this type of webs performed less than the other windowed tubes with CTC webs. Generally, all the windowed tubes absorbed less energy than their standard counterparts, and also they did not provide sufficient reduction for the peak collapsing load.

Funding This research is funded by the Vietnam National Foundation for Science and Technology Development (NAFOSTED) under grant number 107.99-2019.02.

Compliance with ethical standards

Conflict of interest The authors declare that they have no conflict of interest.

Replication of results The parameters that define the design problems have been defined in Section 2.

References

Acar E, Guler MA, Gerçeker B, Cerit ME, Bayram B (2011) Multi-objective crashworthiness optimization of tapered thin-walled tubes with axisymmetric indentations. Thin-Walled Struct 49:94–105

Ahmad Z, Thambiratnam DP (2009) Dynamic computer simulation and energy absorption of foam-filled conical tubes under axial impact loading. Comput Struct 87:186–197

Alavi NA, Parsapour M (2014) Comparative analysis of energy absorption capacity of simple and multi-cell thin-walled tubes with triangular, square, hexagonal and octagonal sections. Thin-Walled Struct 74:155–165

Alkhatib SE, Tarlochan F, Eyvazian A (2017) Collapse behavior of thin-walled corrugated tapered tubes. Eng Struct 150:674–692

Arnold B, Altenhof W (2004) Experimental observations on the crush characteristics of AA6061 T4 and T6 structural square tubes with and without circular discontinuities. Int J Crashworthiness 9:73–87

Baroutaji A, Morris E, Olabi AG (2014) Quasi-static response and multi-objective crashworthiness optimization of oblong tube under lateral loading. Thin-Walled Struct 82:262–277

Baroutaji A, Gilchrist MD, Smyth D, Olabi AG (2015) Crush analysis and multi-objective optimization design for circular tube under quasi-static lateral loading. Thin-Walled Struct 86:121–131

Baroutaji A, Sajjia M, Olabi A-G (2017) On the crashworthiness performance of thin-walled energy absorbers: recent advances and future developments. Thin-Walled Struct 118:137–163

Baroutaji A, Arjunan A, Stanford M, Robinson J, Olabi AG (2021) Deformation and energy absorption of additively manufactured functionally graded thickness thin-walled circular tubes under lateral crushing. Eng Struct 226:111324

Bigdeli A, Nouri MD (2019) A crushing analysis and multi-objective optimization of thin-walled five-cell structures. Thin-Walled Struct 137:1–18

Bodlani SB, Chung Kim Yuen S, Nurick GN (2009a) The energy absorption characteristics of square mild steel tubes with multiple induced circular hole discontinuities—part II: numerical simulations. J Appl Mech 76:041013–041013-10

Bodlani SB, Yuen SCK, Nurick GN (2009b) The energy absorption characteristics of square mild steel tubes with multiple induced circular hole discontinuities—part I: experiments. J Appl Mech 76: 041012–041012

Branke J, Deb K, Dierolf H, Osswald M (2004) Finding knees in multi-objective optimization. In: Yao X, Burke E, Lozano J, Smith J, Merelo-Guervós J, Bullinaria J, Rowe J, Tiňo P, Kabán A, Schwefel H-P (eds) Parallel problem solving from nature - PPSN VIII. Springer, Berlin

Chen W, Wierzbicki T (2001) Relative merits of single-cell, multi-cell and foam-filled thin-walled structures in energy absorption. Thin-Walled Struct 39:287–306

Chen S, Yu H, Fang J (2018) A novel multi-cell tubal structure with circular corners for crashworthiness. Thin-Walled Struct 122:329–343

Dipaolo BP, Monteiro PJM, Gronsky R (2004) Quasi-static axial crush response of a thin-wall, stainless steel box component. Int J Solids Struct 41:3707–3733

El-Hage H, Mallick PK, Zamani N (2005) A numerical study on the quasi-static axial crush characteristics of square aluminum tubes with chamfering and other triggering mechanisms. Int J Crashworthiness 10:183–196

Esa M, Xue P, Zahran M, Abdelwahab M, Khalil M (2017) Novel strategy using crash tubes adaptor for damage levels manipulation and total weight reduction. Thin-Walled Struct 111:176–188

Estrada Q, Szwedowicz D, Gutierrez-Wing E, Silva-Aceves J, Rodriguez-Mendez A, Elias-Espinosa M, Vergara-Vazquez J, Bedolla-Hernandez J (2018a) Energy absorption of single and multi-cell profiles under bending load considering damage evolution. Proc IME D J Autom Eng 233:2120–2138

Estrada Q, Szwedowicz D, Rodriguez-Mendez A, Gómez-Vargas OA, Elias-Espinosa M, Silva-Aceves J (2018b) Energy absorption performance of concentric and multi-cell profiles involving damage evolution criteria. Thin-Walled Struct 124:218–234

Estrada Q, Szwedowicz D, Rodriguez-Mendez A, Elías-Espinosa M, Silva-Aceves J, Bedolla-Hernández J, Gómez-Vargas OA (2019) Effect of radial clearance and holes as crush initiators on the crashworthiness performance of bi-tubular profiles. Thin-Walled Struct 140:43–59

Eyvazian A, Akbarzadeh I, Shakeri M (2012) Experimental study of corrugated tubes under lateral loading. Proc IME L J Mater Des Appl 226:109–118

Eyvazian A, Habibi MK, Hamouda AM, Hedayati R (2014) Axial crushing behavior and energy absorption efficiency of corrugated tubes. Mater Des (1980-2015) 54:1028–1038

Eyvazian A, Tran TN, Hamouda AM (2018) Experimental and theoretical studies on axially crushed corrugated metal tubes. Int J Non-Linear Mech 101:86–94

Eyvazian A, Eltai E, Musharavati F, Taghipoor H, Sebaey TA, Talebizadehsardari P (2020) Experimental and numerical investigations on axial crushing of square cross-sections tube with vertical wave. Steel Compos Struct 36:119–141

Hosseinipour SJ, Daneshi GH (2003) Energy absorbtion and mean crushing load of thin-walled grooved tubes under axial compression. Thin-Walled Struct 41:31–46

Hou S, Li Q, Long S, Yang X, Li W (2007) Design optimization of regular hexagonal thin-walled columns with crashworthiness criteria. Finite Elem Anal Des 43:555–565

Hou S, Li Q, Long S, Yang X, Li W (2008) Multiobjective optimization of multi-cell sections for the crashworthiness design. Int J Impact Eng 35:1355–1367

Hou S, Li Q, Long S, Yang X, Li W (2009) Crashworthiness design for foam filled thin-wall structures. Mater Des 30:2024–2032

Hou S, Han X, Sun G, Long S, Li W, Yang X, Li Q (2011) Multiobjective optimization for tapered circular tubes. Thin-Walled Struct 49:855–863

Hou S, Dong D, Ren L, Han X (2012) Multivariable crashworthiness optimization of vehicle body by unreplicated saturated factorial design. Struct Multidiscip Optim 46:891–905

Hou S, Zhao S, Ren L, Han X, Li Q (2013) Crashworthiness optimization of corrugated sandwich panels. Mater Des 51:1071–1084

Hou S, Zhang Z, Yang X, Yin H, Li Q (2014) Crashworthiness optimization of new thin-walled cellular configurations. Eng Comput 31: 879-897

Kim H-S (2002) New extruded multi-cell aluminum profile for maximum crash energy absorption and weight efficiency. Thin-Walled Struct 40:311–327

Luo Y, Fan H (2018) Energy absorbing ability of rectangular self-similar multi-cell sandwich-walled tubular structures. Thin-Walled Struct 124:88–97

Mahdi Abedi M, Niknejad A, Hossein Liaghat G, Zamani Nejad M (2012) Theoretical and experimental study on empty and foam-filled columns with square and rectangular cross section under axial compression. Int J Mech Sci 65:134–146

Marzbanrad J, Abdollahpoor A, Mashadi B (2009) Effects of the triggering of circular aluminum tubes on crashworthiness. Int J Crashworthiness 14:591–599

Meran AP (2016) Solidity effect on crashworthiness characteristics of thin-walled tubes having various cross-sectional shapes. Int J Crashworthiness 21:135–147

Nguyen N, Yin S, Chen F, Yin H, Pham V, Tran T (2016) Multi-objective optimization of circular magnetic abrasive polishing of SUS304 and Cu materials. J Mech Sci Technol 30:2643–2650

Nguyen N, Tran T, Yin S, Chau M, Le D (2017) Multi-objective optimization of improved magnetic abrasive finishing of multi-curved surfaces made of SUS202 material. Int J Adv Manuf Tech 88:381–391

Nikkhah H, Baroutaji A, Olabi AG (2019) Crashworthiness design and optimisation of windowed tubes under axial impact loading. Thin-Walled Struct 142:132–148

Nikkhah H, Baroutaji A, Kazanc Z, Arjunan A (2020) Evaluation of crushing and energy absorption characteristics of bio-inspired nested structures. Thin-Walled Struct 148:106615

Niknejad A, Bonakdar S (2015) A new theoretical analysis for the splitting of square columns subjected to the axial loading. Sci Iran 22: 804–812

Niknejad A, Orojloo PH (2016) A novel nested system of tubes with special cross-section as the energy absorber. Thin-Walled Struct 100:113–123

Santosa SP, Wierzbicki T, Hanssen AG, Langseth M (2000) Experimental and numerical studies of foam-filled sections. Int J Impact Eng 24:509–534

Shen W, Gu X, Jiang P, Hu J, Lv X, Qian L (2017) Crushing analysis and multiobjective optimization design for rectangular unequal triple-cell tubes subjected to axial loading. Thin-Walled Struct 117:190–198

Sun G, Li G, Zhou S, Li H, Hou S, Li Q (2011) Crashworthiness design of vehicle by using multiobjective robust optimization. Struct Multidiscip Optim 44:99–110

Sun G, Xu F, Li G, Li Q (2014) Crashing analysis and multiobjective optimization for thin-walled structures with functionally graded thickness. Int J Impact Eng 64:62–74

Sun G, Pang T, Xu C, Zheng G, Song J (2017) Energy absorption mechanics for variable thickness thin-walled structures. Thin-Walled Struct 118:214–228

Taghipoor H, Damghani Nouri M (2018a) Axial crushing and transverse bending responses of sandwich structures with lattice core. J Sandw Struct Mater 22:572–598

Taghipoor H, Damghani Nouri M (2018b) Experimental and numerical investigation of lattice core sandwich beams under low-velocity bending impact. J Sandw Struct Mater 21:2154–2177

Taghipoor H, Noori Mohammad D (2018) Experimental and numerical study on energy absorption of lattice-core sandwich beam. Steel Compos Struct 27:135–147

Taghipoor H, Eyvazian A, Ghiaskar A, Praveen Kumar A, Magid Hamouda A, Gobbi M (2020a) Experimental and numerical study of lattice-core sandwich panels under low-speed impact. Mater Today Proc 27:1487–1492

Taghipoor H, Eyvazian A, Ghiaskar A, Praveen Kumar A, Magid Hamouda A, Gobbi M (2020b) Experimental investigation of the thin-walled energy absorbers with different sections including surface imperfections under low-speed impact test. Mater Today Proc 27:1498–1504

Tran T, Baroutaji A (2018) Crashworthiness optimal design of multi-cell triangular tubes under axial and oblique impact loading. Eng Fail Anal 93:241–256

Tran T, Hou S, Han X, Nguyen N, Chau M (2014) Theoretical prediction and crashworthiness optimization of multi-cell square tubes under oblique impact loading. Int J Mech Sci 89:177–193

Tran T, Le D, Baroutaji A (2019) Theoretical and numerical crush analysis of multi-stage nested aluminium alloy tubular structures under axial impact loading. Eng Struct 182:39–50

Tran T, Eyvazian A, Estrada Q, Le D, Nguyen N, Le H (2020) Lateral behaviors of nested tube systems under quasi-static condition. Int J Appl Mech 12:2050046

Vimal Kannan I, Rajkumar R (2020) Deformation and energy absorption analysis of simple and multi-cell thin-walled tubes under quasi-static axial crushing. Int J Crashworthiness 25:121–130

Xu X, Zhang Y, Wang J, Jiang F, Wang CH (2018) Crashworthiness design of novel hierarchical hexagonal columns. Compos Struct 194:36–48

Yang K, Xu S, Zhou S, Xie YM (2018) Multi-objective optimization of multi-cell tubes with origami patterns for energy absorption. Thin-Walled Struct 123:100–113

Yin H, Wen G, Liu Z, Qing Q (2014) Crashworthiness optimization design for foam-filled multi-cell thin-walled structures. Thin-Walled Struct 75:8–17

Yin H, Fang H, Xiao Y, Wen G, Qing Q (2015) Multi-objective robust optimization of foam-filled tapered multi-cell thin-walled structures. Struct Multidiscip Optim 52:1051–1067

Yin H, Wen G, Bai Z, Chen Z, Qing Q (2017). Theoretical prediction and crashworthiness optimization of multi-cell polygonal tubes. J Sandw Struct Mater 22:190–219

Yin H, Wen G, Bai Z, Chen Z, Qing Q (2020) Theoretical prediction and crashworthiness optimization of multi-cell polygonal tubes. J Sandw Struct Mater 22:190–219

Zahran MS, Xue P, Esa MS, Abdelwahab MM (2018) A novel tailor-made technique for enhancing the crashworthiness by multi-stage tubular square tubes. Thin-Walled Struct 122:19

Zhang L, Bai Z, BAI F (2018) Crashworthiness design for bio-inspired multi-cell tubes with quadrilateral, hexagonal and octagonal sections. Thin-Walled Struct 122:42–51